Darcy-Forchheimer flow of Maxwell nanofluid flow with nonlinear thermal radiation and activation energy

Cite as: AIP Advances **8**, 035102 (2018); https://doi.org/10.1063/1.5019218
Submitted: 12 December 2017 • Accepted: 12 February 2018 • Published Online: 01 March 2018

T. Sajid, M. Sagheer, S. Hussain, et al.

Darcy-Forchheimer flow of Maxwell nanofluid flow with nonlinear thermal radiation and activation energy

T. Sajid,[a] M. Sagheer, S. Hussain, and M. Bilal
Department of Mathematics, Capital University of Science and Technology, Islamabad 46000, Pakistan

(Received 12 December 2017; accepted 12 February 2018; published online 1 March 2018)

The present article is about the study of Darcy-Forchheimer flow of Maxwell nanofluid over a linear stretching surface. Effects like variable thermal conductivity, activation energy, nonlinear thermal radiation is also incorporated for the analysis of heat and mass transfer. The governing nonlinear partial differential equations (PDEs) with convective boundary conditions are first converted into the nonlinear ordinary differential equations (ODEs) with the help of similarity transformation, and then the resulting nonlinear ODEs are solved with the help of shooting method and MATLAB built-in bvp4c solver. The impact of different physical parameters like Brownian motion, thermophoresis parameter, Reynolds number, magnetic parameter, nonlinear radiative heat flux, Prandtl number, Lewis number, reaction rate constant, activation energy and Biot number on Nusselt number, velocity, temperature and concentration profile has been discussed. It is viewed that both thermophoresis parameter and activation energy parameter has ascending effect on the concentration profile.
https://doi.org/10.1063/1.5019218

NOMENCLATURE

a, c	constants
C	nanoparticles concentration
C_w	skin friction
C_∞	ambient concentration
D_B	Brownian diffusion coefficient
λ_1	relaxation time
M	magnetic parameter
γ	Biot number
λ	porosity parameter
j_w	mass flux
Le	Lewis number
N_b	Brownian motion parameter
Nu_x	Nusselt number
Pr	Prandtl number
E_a	activation energy
σ	reaction rate constant
n	fitted rate constant
B_0	magnetic field strength
T_w	convective fluid temperature
σ^*	Stefan-Boltzman constant

[a]Corresponding author e-mail address: tanveer.sajid15@yahoo.com

$(\rho c)_p$	heat capacity of nanoparticles
h_f	heat transfer coefficient
ϵ	thermal conductivity parameter
T	temperature of fluid
T_∞	ambient temperature
(u, v)	velocity components
D_T	thermophoretic diffusivity
$u_w(x)$	velocity of the stretching surface
F_r	inertia coefficient
α	thermal diffusivity
β	Deborah number
κ	temperature dependent thermal conductivity
q_w	surface heat flux
N_t	thermophoresis parameter
ϕ	dimensionless concentration
Rd	radiation parameter
Sc	Schmidt number
δ	temperature difference parameter
q_r	radiative heat flux
θ_w	temperature ratio parameter
μ	dynamic viscosity
κ^*	absorption coefficient
$(\rho c)_f$	heat capacity of fluid
T_f	temperature of hot fluid

I. INTRODUCTION

Type of material having pores is called porous media, where the pores are usually filled with fluid. The concept of fluid flow in porous media is of great interest for engineers, mathematicians, geologists and architectures due to its diverse applications, like the flow of water in reservoirs, heat exchanger, oil production and catalytic reactors etc. The process of heat transfer in porous media has abundantly been used in the production of papers, non-woven materials, heat pipe technology, electronic technology and energy storage etc.[1–4] In 1856, Henry Darcy, a French civil engineer, laid the foundation of flow of homogeneous fluids through porous media during his work on flow of water through sand beds. Darcy law cannot work well when inertial and boundary effects take place at higher flow rate. Later on, in 1901, Philippes Forchheimer, a Dutch scientist, extended the Darcian velocity expression by adding the square velocity term in the momentum equation for the prediction of the behavior of inertia and boundary layer flow.[5] The name 'Forchheimer term' was later coined by Muskat.[6] Pal and Mondal[7] considered the Darcy-Forchheimer model over stretching surface and concluded that an increase in the value of electric field parameter results in decreasing the nanoparticle concentration profile. Ganesh et al.[8] worked on the Darcy-Forchheimer MHD nanofluid flow over stretching/shrinking sheet and explored that the temperature profile increases in the presence of viscous dissipation effect. Hayat et al.[9] worked on the Darcy-Forchheimer flow of Maxwell fluid, subjected to the thermal conductivity and Cattaneo-Christov expression. They observed that both the thermal boundary layer thickness and the temperature profile decrease by increasing the Prandtl number. Recent work of Muhammad et al.[10] on the Darcy-Forchheimer Maxwell nanofluid subjected to the convective and zero mass flux boundary conditions over a stretching sheet, using porous media, lead to the fact that, by enhancing the value of porosity parameter results in an increase of the temperature and nanoparticle concentration profile. Ahmed et al.[11] contemplated the Jeffery fluid past a stretching sheet along with MHD and convective boundary condition. They found that the temperature profile decreases due to an increment in the Biot number. Alsaedi et al.[12] found the numerical solution of Burgers' fluid flow over a shrinking surface with stagnation point and chemical reaction. They noticed that a decrement in the concentration field happens due to an augmentation

in the Schmidt number. Aziz et al.[13] numerically treated the unsteady flow of third grade fluid past a flat porous plate embedded in a porous medium with the help of homotopy analysis method (HAM) and found that the velocity profile decreases with an enhancement in the material parameter. They also noticed a decrement in the concentration field due to an augmentation in the Schmidt number. Shahzad et al.[14] found the exact solution of MHD viscous fluid flow towards a nonlinear radially stretching sheet embedded in a porous medium and noticed that an abatement in the temperature field occurs due to an escalation in the material parameter.

In the present era, the cooling process is a much needed phenomenon in terms of applications to mitigate heating effects in computer chips, car engines etc. In past, the conventional liquids like water, oil, ethylene glycol were used for controlling the heat effects. Later on, a new technique containing solid-liquid mixture of nanoparticles and base liquid, named as nanofluid, was introduced by Choi,[15] with lot of applications in biomedical, optical, electronics and ceramic industry. The heat absorption tendency of nanofluids is much higher than that of the traditional liquids. Research on nanoparticles by Das et al.,[16] Wang and Mujumdar,[17] Usria et al.[18] and Murshed et al.[19] has concluded that mixing of nanoparticles with liquids enhances the thermal conductivity. Buongiorno[20] developed a model with Brownian motion and thermophoresis aspects. He affirmed that abnormality in heat transfer occurs due to the movement of particles in a fluid. He presented a seven parameters regarding slip mechanisms to generate a parallel velocity between the nanoparticles and base fluid. These seven parameters are inertia, thermophoresis, magnus effect, gravity, fluid drainage, Brownian diffusion and diffusiophoresis. Furthermore, he introduced a model including the Brownian motion and thermophoresis terms in the energy equation for convention in nanofluids. Recently Oyelakin[21] investigated unsteady the Casson nanofluid with thermal radiation and observed that an increase in the heat generation parameter results in the decrease in temperature profile. Hayat et al.[22] worked on the Carreau nanofluid with convective boundary over stretching sheet, deliberating on effects of Brownian motion and thermophoresis parameter. Some more relevant articles has been cited in Refs. 23–26.

Magnetohydrodynamics (MHD) is a study of magnetic effects in electrically conducting fluids. MHD has immense involvement in processes like earth magnetic field, solar wind, fusion, cooling of fission reactors, star formation, tumor therapy, X-ray radiation, plasmas, electrolytes etc. Kothandapani and Prakash[27] adopted the homotopy perturbation method to study the convective boundary conditions on peristaltic flow of a Jeffery nanofluid and observed that the volume of trapped channel decreases with an increase in the chemical reaction. Ullah et al.[28] used the Keller box method scheme to study the MHD Casson fluid over the nonlinear stretching sheet. Shehzad et al.[29] discussed the MHD flow of nanofluid by HAM with convective mass condition. They observed that an increase in the Biot number causes an increase in both temperature and concentration profiles. Hayat et al.,[30] with the help of HAM, discussed the MHD flow of viscous incompressible nanofluid over a stretching sheet in the presence of magnetic field and convective boundary condition. Ibrahim[31] presented an analysis of the stagnation point flow and heat transfer of upper-convected Maxwell fluid on a moving vertical porous plate with induced magnetic field and linear thermal radiation effects. MHD incompressible flow of coupled stress fluid over a rotating disk was discussed by Khan et al.[32] They concluded that the magnetic field opposes the fluid velocity in all directions. Rauf et al.[33] discussed the flow of nanofluid in the presence of convective and mass flux condition. They noticed that the concentration profile decreases with an increase in the Schmidt number. Ali et al[34] employed both the homotopical analysis method and the shooting technique to work out the solution of MHD viscous fluid subject to the partial slip condition. They concluded that a reduction in the velocity field happens because of an embellishment in the slip parameter.

Radiative heat transfer is caused by the electromagnetic radiation. Radiation does not require any medium for prorogation but depends on the factors like temperature, solid geometric arrangement, surface properties of the material that are emitting or absorbing heat. It is quite clear that when temperature difference is high/low, the radiation transmission between two bodies is intensified/declined. In industry it is troublesome to design a system with fluid flow inside the system having small temperature difference. Due to this difficulty researcher lately presented the nonlinear thermal radiation with addition of extra parameter as compared to linear thermal radiation. This extra parameter indicates the difference between wall temperature and ambient temperature. In the presence of high

temperature difference, the radiation transfer between two bodies is strengthened. For an appropriate brief literature survey on this topic, articles cited in Refs. 35–39 can be consulted.

Different fields of science like chemical engineering, geo-thermal reservoirs, oil emulsions, food processing, mechano chemistry involve mass transfer phenomenon carried out by chemical reaction and activation energy. The mass transfer occurs due to concentration difference of species present in a mixture. The species with changing concentration in a mixture carry themselves from the state of higher concentration to the state of lower concentration. Activation energy is defined as the minimum amount of energy owned by a reacting specie to undergo an indicated reaction. The Arrhenius equation is usually of the form[40]

$$K = B\left(\frac{T}{T_\infty}\right)^n \exp\left(\frac{-E_a}{\kappa T}\right), \tag{1}$$

where K represents reaction rate constant, Ea is the activation energy, T the fluid temperature and B the pre-exceptional factor depicting an increase in the temperature with respect to increase in the reaction rate. Before 1990, no attention was given to the effect of activation energy on mass flow. However, in 1990, Bestman[41] worked on the effect of Arrhenius activation energy in the heat and mass transfer in a porous medium. After that Abdul Maleque[42] studied the effect of activation energy on an unsteady free convective flow of heat and mass transfer. He noticed that the velocity profile increases by increasing the value of the Greshof number. Recently Shafique et al.[43] deliberated the rotating flow of Maxwell fluid in the context of heat and mass transfer over a stretching surface with activation energy and binary chemical reaction. Mustafa et al.,[44] after examining the behaviour of binary chemical reaction and activation energy in the MHD viscoelastic fluid flow over linearly stretching sheet, observed that the concentration profile escalates by escalating the value of activation energy.

The characteristic of a substance to conduct heat is called thermal conductivity. Thermal conductivity changes dramatically with a change in temperature. Once the effects of thermal conductivity are considered in mathematical modeling, it is easy to predict the fluid behaviour. For example, if we consider a lubricating fluid, the frictional forces enhance the temperature of the fluid. Vajravelu et al.[45] investigated the viscous fluid flow over a vertical plate with convective boundary condition and fluid flow properties. They examined that the thermal boundary layer is thicker in the presence of suction parameter. Kumar and Sivaraj[46] analyzed the flow of heat transfer in viscous fluid passing a vertical cone over a flat plate. They concluded that by increasing the value of Eckart number, an increment in both the velocity and temperature profiles is observed. Mixed convection MHD flow over a stretching sheet with thermal conduction was discussed by Pal and Mondal.[47] They investigated that an increment in the Schmidt number leads to the decrement in the concentration profile. Pal and Chatterjee[48] discussed the MHD mixed convection flow of power-law fluid over an inclined plate with variable thermal conductivity, chemical reaction, thermal radiation, suction/injection and Ohmic dissipation.

With reference to the literature discussed above, the task in this paper is to investigate the MHD Maxwell nanofluid through Darcy-Forchheimer porous medium in the presence of the convective boundary condition and zero mass flux condition with the assumption of activation energy. nonlinear thermal radiation and variable thermal conductivity. To the best of our knowledge, the Darcy-Forchheimer flow of Maxwell nanofluid over a linear stretching surface with variable thermal conductivity, radiative heat flux and activation energy has not been investigated yet.

II. MATHEMATICAL FORMULATION

Consider two dimensional incompressible Maxwell nanofluid embedded in a non Darcy-porous medium with fluid flow generated due to linear stretching sheet. Sheet is stretching along x-axis and normal to y-axis. Magnetic field B_0 is applied perpendicular to sheet. Reynolds number is considered very small so that the effect of induced magnetic field current can be neglected. The stretching surface velocity is $u_w(x) = ax$ along x axis. Temperature is regulated by the convective heating process described by the heat transfer coefficient h_f and the temperature of the hot fluid T_f under the

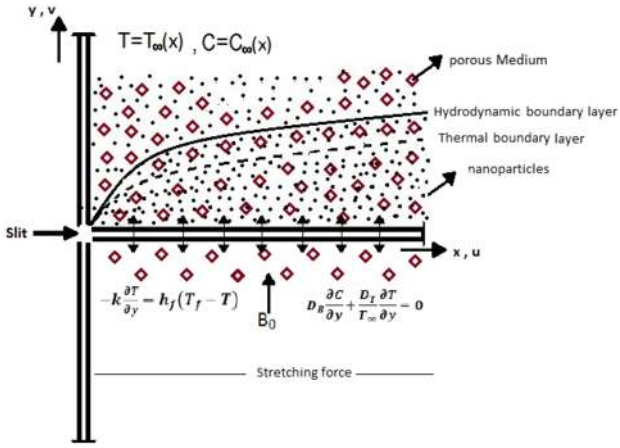

FIG. 1. Geometry of the Problem.

sheet as shown in Fig. 1. By using the boundary layer approximation, the governing nonlinear PDEs are

$$\frac{\partial u}{\partial x}+\frac{\partial v}{\partial y}=0, \tag{2}$$

$$u\frac{\partial u}{\partial x}+v\frac{\partial u}{\partial y}+\lambda_1\left(\begin{matrix}u^2\frac{\partial^2 u}{\partial x^2}+v^2\frac{\partial^2 u}{\partial y^2}\\ +2uv\frac{\partial^2 u}{\partial x\partial y}\end{matrix}\right)=\nu\frac{\partial^2 u}{\partial y^2}-\frac{\sigma_1 B_0^2}{\rho_f}\left(u+\lambda_1 v\frac{\partial u}{\partial y}\right)-\frac{\nu}{K}u-Fu^2, \tag{3}$$

$$u\frac{\partial T}{\partial x}+v\frac{\partial T}{\partial y}=\frac{1}{\rho c_p}\frac{\partial}{\partial y}\left(\kappa\frac{\partial T}{\partial y}\right)+\tau\left[D_B\frac{\partial C}{\partial y}\frac{\partial T}{\partial y}+\frac{D_T}{T_\infty}\left(\frac{\partial T}{\partial y}\right)^2\right]-\frac{1}{\rho c_p}\frac{\partial q_r}{\partial y}, \tag{4}$$

$$u\frac{\partial C}{\partial x}+v\frac{\partial C}{\partial y}=D_B\left(\frac{\partial^2 C}{\partial y^2}\right)+\frac{D_T}{T_\infty}\left(\frac{\partial^2 T}{\partial y^2}\right)-K_r^2(C-C_\infty)\left(\frac{T}{T_\infty}\right)^n\exp\left(\frac{-E_a}{\kappa T}\right), \tag{5}$$

along with the boundary conditions

$$\left.\begin{aligned}&y=0: u=u_w(x)=ax, v=0, -k\frac{\partial T}{\partial y}=h_f(T_w-T),\ D_B\frac{\partial C}{\partial y}+\frac{D_T}{T_\infty}\frac{\partial T}{\partial y}=0,\\ &y\to\infty: u\to 0,\ T\to T_\infty,\ C\to C_\infty,\end{aligned}\right\} \tag{6}$$

where $F=\frac{C_b}{xK^{\frac{1}{2}}}$ is the inertia coefficient.

Temperature dependent thermal conductivity is expressed as

$$\kappa=\kappa_\infty\left(1+\epsilon\frac{T-T_\infty}{T_w-T_\infty}\right). \tag{7}$$

Rosseland approximation for radiation is

$$q_r=-\frac{4\sigma^*}{3\kappa^*}\frac{\partial T^4}{\partial y}. \tag{8}$$

terms σ^* and κ^* in the above equation represent the constants known as Stefan-Boltzmann constant and the mean absorption coefficient respectively. From (8), after simplification, we get

$$\frac{\partial q_r}{\partial y}=-\frac{16\sigma^* T_\infty^3}{3\kappa^*}\frac{\partial^2 T}{\partial y^2}. \tag{9}$$

In the concentration equation, the term $K_r^2(C-C_\infty)\left(\frac{T}{T_\infty}\right)^n\exp\left(\frac{-E_a}{\kappa T}\right)$ represents the Arrhenius expression, where K_r^2 is the reaction rate.

To convert PDEs to ODEs, we adopt the following similarity transformation:[22,26,29]

$$u = axf'(\eta),\ v = -\sqrt{av}f(\eta),\ \eta = \sqrt{\frac{a}{\nu}}y,\ \phi(\eta) = \frac{C - C_\infty}{C_w - C_\infty},\ \theta(\eta) = \frac{T - T_\infty}{T_w - T_\infty}. \tag{10}$$

The continuity equation is satisfied automatically and Eqs. (2)–(6) are converted into the following non-dimensional form:

$$f''' + \left(M^2\beta + 1\right)ff'' + \beta\left(2ff'f'' - f^2f'''\right) - \left(M^2 + \lambda\right)f' - (1 + F_r)f'^2 = 0, \tag{11}$$

$$((1 + \epsilon\theta) + \frac{4}{3}Rd\,(1 + (\theta_w - 1)\,\theta)^3)\theta'' + \left(\epsilon + 4Rd\,(\theta_w - 1)\,(1 + (\theta_w - 1)\,\theta)^2\,\theta'^2\right) + Prf\theta' + Pr(N_b\theta'\phi' + N_t\theta'^2) = 0, \tag{12}$$

$$\phi'' + \left(\frac{Nt}{Nb}\right)\theta'' + PrLef\phi' - PrLe\,\sigma\,(1 + \delta\theta)^n \exp\left(\frac{-E}{1 + \delta\theta}\right)\phi = 0, \tag{13}$$

The dimensionless form of the boundary conditions is

$$\left.\begin{aligned} &\eta = 0 : f(\eta) = 0, \quad f'(\eta) = 1, \quad \theta'(\eta) = -\gamma(1 - \theta(\eta)), \quad Nb\theta'(\eta) + Nt\phi'(\eta) = 0, \\ &\eta \to \infty : f'(\eta) \to 0, \quad \theta(\eta) \to 0, \quad \phi(\eta) \to 0. \end{aligned}\right\} \tag{14}$$

Different dimensionless parameters appearing in equations Eqs. (10)–(14) are defined as

$$\left.\begin{aligned} &Re_x = \frac{u_e(x)x}{\nu}, \quad b = a/c, \quad E = \left(\frac{E_a}{\kappa T_\infty}\right), \quad \delta = \frac{T_w - T_\infty}{T_\infty} \\ &\beta = \lambda_1 a, \quad \lambda = \frac{\nu}{Ka}, \quad Pr = \frac{\nu}{\alpha}, \quad Le = \frac{\alpha}{D_B}, \quad \gamma = \frac{h}{k}\sqrt{\frac{\nu}{c}}, \\ &Nb = \frac{\tau D_B}{\nu}(C_w - C_\infty), \quad Nt = \frac{D_T}{T_\infty}\frac{\tau}{\nu}(T_w - T_\infty), \quad F_r = \frac{C_b}{K^{\frac{1}{2}}}, \\ &R_d = \frac{4\sigma T_\infty^3}{k^* k_\infty}, \quad \sigma = \frac{k_r^2}{c}, \quad \tau = \frac{\rho C_p}{\rho C_f} \end{aligned}\right\} \tag{15}$$

The local Nusselt number is formulated as

$$Nu_x = \frac{xq_w}{k(T_w - T_\infty)}, \tag{16}$$

where the heat flux q_w is given by

$$q_w = -k\left(\frac{\partial T}{\partial y}\right)_{y=0} + \ q_r. \tag{17}$$

The dimensionless form of Nusselt number is given by

$$Nu_x Re_x^{-1/2} = -\left(1 + \frac{4}{3}Rd\,((\theta_w - 1)\theta(0) + 1)^3\right)\theta'(0). \tag{18}$$

III. SOLUTION METHODOLOGY

The nonlinear non-dimensional transformed problem (11)–(13) along with the boundary conditions (14) has been solved with the help of the shooting method.[49,50] For confirmation of the upcoming results, the problem is also tackled with the help of the MATLAB built-in bvp4c solver. To solve the problem numerically, we consider the domain of the problem [0, 7] instead of [0, ∞]. To convert the boundary value problem into an initial value problem comprising of a system of seven first order

ODEs, let us denote f by y_1, θ by y_4 and ϕ by y_6. The resulting equations are

$$\left.\begin{aligned}
y_1' &= y_2,\\
y_2' &= y_3,\\
y_3' &= \left(\frac{1}{1-\beta y_1^2}\right)\left[\left(M^2+\lambda\right)y_2 + (1+F_r)\,y_2^2 - \left(M^2\beta+1\right)y_1y_3 - 2\beta y_1y_2y_3\right],\\
y_4' &= y_5,\\
y_5' &= -\frac{1}{\left((1+\epsilon y_4)+\frac{4}{3}Rd\,(1+(\theta_w-1)\,y_4)^3\right)}\left[\begin{array}{c}(\epsilon+4Rd(\theta_w-1)(1+(\theta_w-1)y_4)^2y_5^2\\ +Prfy_1y_5 + Pr\left(Nby_5y_7 + Nt\,y_5^2\right)\end{array}\right],\\
y_6' &= y_7,\\
y_7' &= PrLe\;\sigma\,(1+\delta y_4)^n \exp\left(\frac{-E}{1+\delta y_4}\right)y_6 - PrLey_1y_7 - \left(\frac{Nt}{Nb}\right)y_5',
\end{aligned}\right\} \tag{19}$$

subject to the boundary conditions

$$\left.\begin{aligned}
&\eta = 0:\; y_1(0)=0,\; y_2(0)=1,\; y_3(0)=\xi_1,\; y_4(0)=\xi_2,\; y_5(0)=-\gamma\,(1-\xi_2),\\
&y_6(0)=\xi_3,\; y_7(0)=\frac{Nb}{Nt}\gamma\,(1-\xi_2).\\
&\eta\to\infty:\; y_2(\infty)\to 0,\; y_4(\infty)\to 0,\; y_6(\infty)\to 0.
\end{aligned}\right\} \tag{20}$$

For some appropriate choice of the missing initial conditions ξ_1, ξ_2 and ξ_3, the IVP is solved by the RK4 method. With the help of the Newton's method, the values of s, t and u are improved until the criteria given below is satisfied.

$$\max\{|y_2(7)|, |y_4(7)|, |y_6(7)\} < \varepsilon, \tag{21}$$

where $\varepsilon > 0$ represents any positive number. The numerical results in this paper are achieved with $\varepsilon = 10^{-6}$.

IV. RESULTS AND DISCUSSIONS

In Table I the present results for Nusselt number are compared with those obtained by Muhammad et al.[10] for different parameters, which shows a very good agreement. Through Table II increase in the wall thickness parameter α, linear thermal radiation Rd, Prandtl number Pr results an increase in the Nusselt number, whereas by increasing the values of the magnetic parameter M, thermal conductivity ϵ, thermophoresis parameter N_t, Lewis number Le, a decrease in the Nusselt number is observed. From Table III it can be seen that an enhancement in the Deborah number β, reaction rate constant σ, fitted rate constant n, porosity parameter λ, temperature difference parameter δ leads to an increase in the Nusselt number.

The impact of Deborah number on the velocity profile is shown in Fig. 2. It can be seen that the velocity profile decreases by increasing the value of Deborah number. Deborah number is actually determines the difference amongst solids and fluids. On account of smaller Deborah number the material responds like fluid however inverse on account of large value of Deborah number where material acts like a solids. Both velocity profile and the boundary layer thickness decreases and approaches to zero by augmenting the value of Deborah number. As a result velocity profile decreases. Fig. 3 shows that an increase in the inertia coefficient leads to a decreases in the velocity profile. It is found that by increasing the inertia coefficient, the thermal boundary layer becomes more thick and fluid cannot move easily. Fig. 4 demonstrates the variation of the velocity profile for different values of the porosity parameter. It is observed that when we increase the porosity parameter, the velocity profile decreases. Fig. 5 demonstrates the variation of the velocity profile with respect to the magnetic parameter M. When we increase the magnetic parameter M, the velocity profile decreases because of the magnetic field. An electrically conducting fluid, in the presence of magnetic field generates a force known as the Lorentz force. Collision of molecules increases in the presence of Lorentz

TABLE I. Comparison of the local Nusselt number $-\theta'(0)$ by the shooting method and bvp4c with those of Muhammad et al.[10] for different values of β, M, λ, F_r, Le, Pr, γ, N_t.

β	M	λ	Fr	Le	Pr	γ	N_t	Ref. 10	Shooting	bvp4c
0.0								0.20321	0.20325	0.20325
0.5								0.19945	0.19955	0.19955
1.0								0.19587	0.19606	0.19606
	0.0							0.20178	0.20185	0.20185
	0.5							0.19954	0.19939	0.19939
	0.8							0.19633	0.19592	0.19592
		0.0						0.20358	0.20361	0.20361
		0.4						0.19990	0.19999	0.19999
		0.8						0.19656	0.19676	0.19676
			0.0					0.20203	0.20207	0.20207
			0.5					0.20042	0.20050	0.20050
			1.0					0.19895	0.19905	0.19905
				0.5				0.20203	0.20188	0.20188
				1.0				0.20169	0.20175	0.20175
				1.5				0.20160	0.20166	0.20166
					0.5			0.15592	0.15955	0.15955
					1.0			0.19306	0.19326	0.19326
					1.5			0.21147	0.21146	0.21146
						0.2		0.15100	0.15103	0.15103
						0.7		0.32691	0.32708	0.32708
						1.2		0.40532	0.40559	0.40559
							0.0	0.20204	0.20120	0.20120
							0.5	0.20022	0.20028	0.20028
							1.0	0.19828	0.19883	0.19883

force. Due to this temperature of fluid rises and as a result reduction in the fluid velocity takes place within the boundary layer. Fig. 6 represents the fact that when the Deborah number increases both the temperature profile and thermal boundary layer thickness increase. The influence of the variable

TABLE II. Values of the local Nusselt number for different parameters.

							$Nu_x Re_x^{\frac{-1}{2}}$	
M	Rd	θ_w	ϵ	N_t	Pr	Le	Shooting	bvp4c
0.2							0.288567	0.288567
0.4							0.286350	0.286350
0.6							0.282915	0.282915
0.7							0.280399	0.280399
	0.5						0.315386	0.315386
	0.6						0.341821	0.341821
	0.7						0.367946	0.367946
		1.6					0.301540	0.301540
		1.7					0.315907	0.315907
		1.8					0.331768	0.331768
			0.3				0.285396	0.285396
			0.4				0.282241	0.282241
			0.5				0.279105	0.279105
				0.9			0.287217	0.287217
				1.0			0.285850	0.285850
				1.2			0.283961	0.283961
					1.2		0.303084	0.303084
					1.4		0.315554	0.315554
					1.6		0.326182	0.326182
						1.2	0.288249	0.288249
						1.4	0.287996	0.287996
						1.6	0.287789	0.287789

TABLE III. Values of the local Nusselt number for different parameters.

								$Nu_x Re_x^{\frac{-1}{2}}$	
E	σ	n	δ	β	λ	F_r	γ	Shooting	bvp4c
0.3								0.288891	0.288891
0.5								0.289222	0.289222
0.7								0.289553	0.289553
	1.2							0.288281	0.288281
	1.4							0.288048	0.288048
	1.5							0.287947	0.287947
		0.5						0.304049	0.304049
		0.7						0.304031	0.304031
		0.9						0.304011	0.304011
			1.8					0.288389	0.288389
			2.0					0.288156	0.288156
			2.2					0.288048	0.288048
				0.4				0.285732	0.285732
				0.6				0.283048	0.283048
				0.8				0.280507	0.280507
					1.0			0.285352	0.285352
					1.2			0.282384	0.282384
					1.4			0.279635	0.279635
						0.3		0.287491	0.287491
						0.5		0.286455	0.286455
						0.7		0.285455	0.285455
							0.5	0.360750	0.360750
							0.7	0.399335	0.399335
							0.9	0.422897	0.422897

thermal conductivity parameter on the temperature profile has been discussed in Fig. 7. The influence of the variable thermal conductivity parameter ϵ is to increase the temperature profile meaningfully but reverse in the case of the volume fraction nanoparticles, thats why the cooling rate is more faster for the coolant having small thermal conductivity parameter. Fig. 8 displays the relationship between the inertia coefficient and the temperature profile. An increase in the inertia coefficient leads to a strong temperature profile and boundary layer thickness. Fig. 9 is portrayed to analyze the relationship between the porosity parameter and the temperature profile. The temperature profile and the thermal layer thickness increase as the porosity parameter increases. It is noticed that the presence of porous

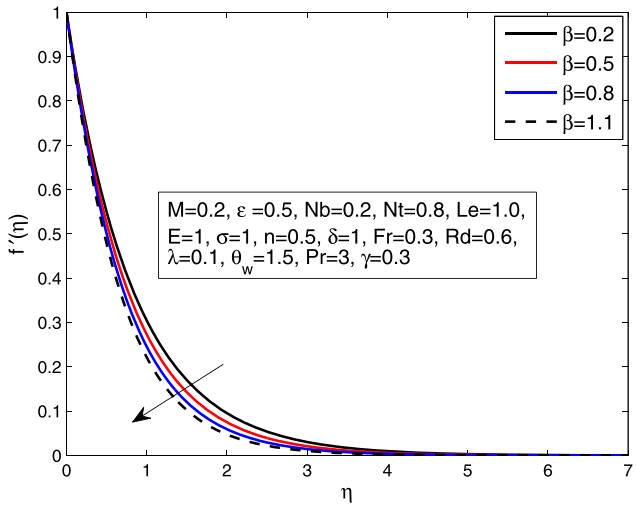

FIG. 2. Influence of β on $f^{'}$.

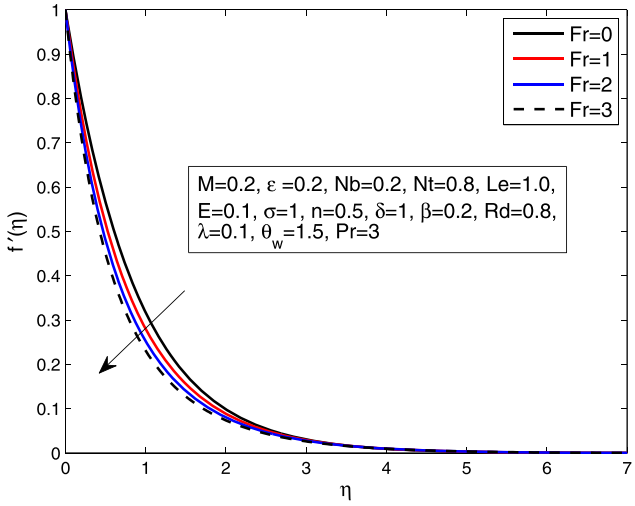

FIG. 3. Influence of Fr on $f^{'}$.

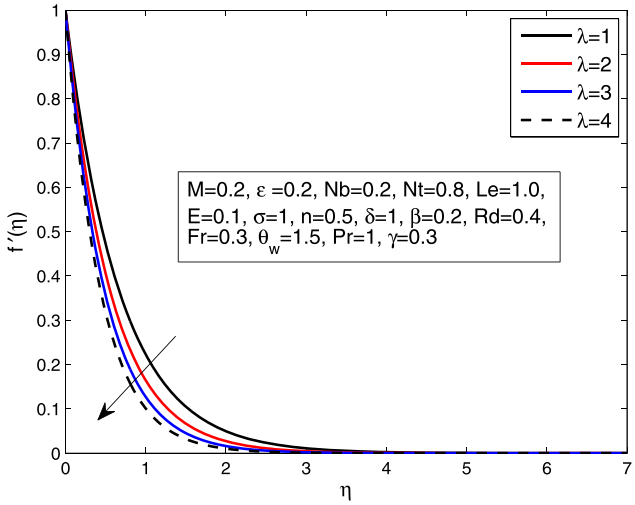

FIG. 4. Influence of λ on $f^{'}$.

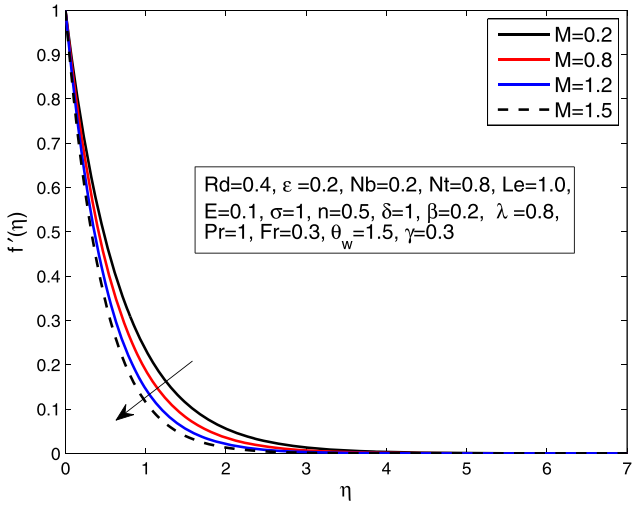

FIG. 5. Influence of M on $f^{'}$.

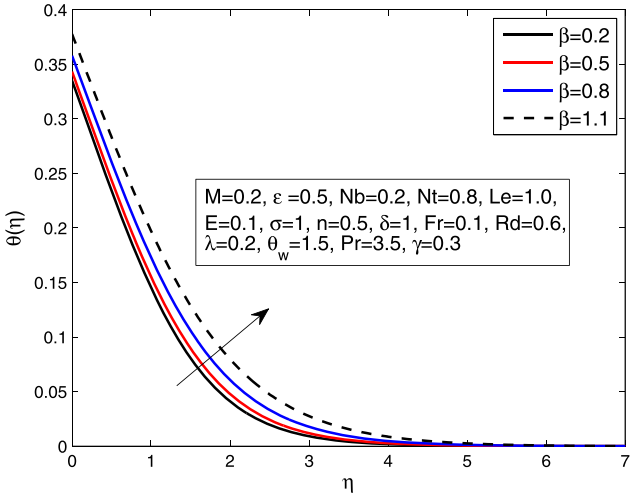

FIG. 6. Influence of β on θ.

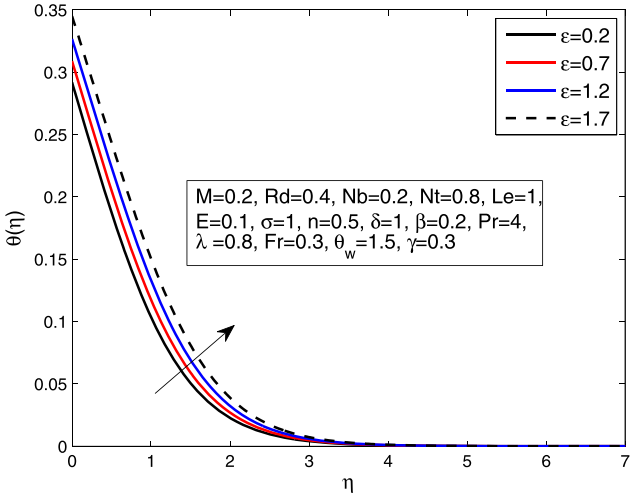

FIG. 7. Influence of ϵ on θ.

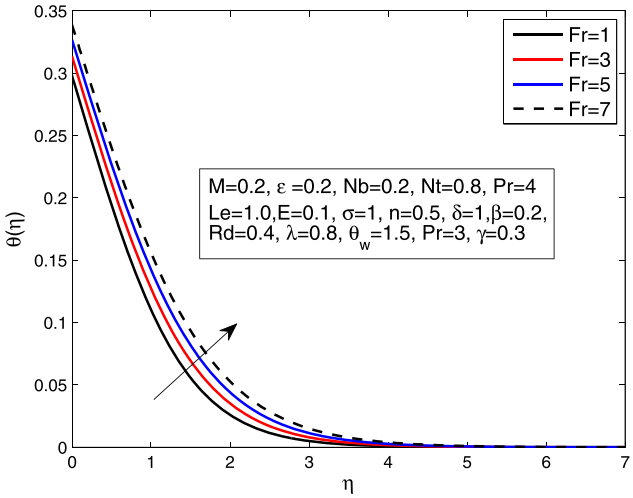

FIG. 8. Influence of Fr on θ.

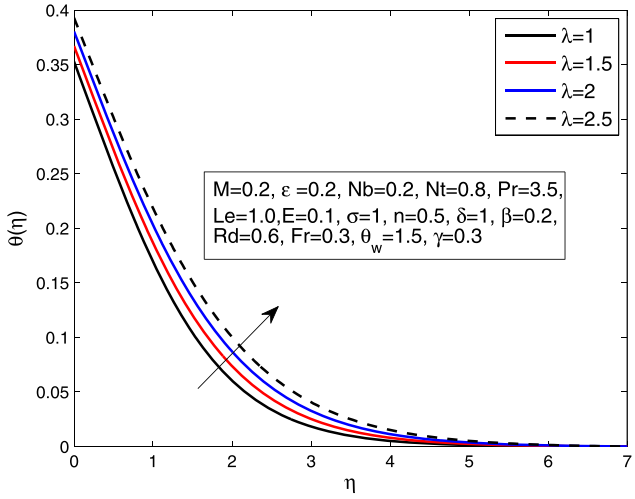

FIG. 9. Influence of λ on θ.

media creates an increment in the resistance against the fluid flow which ultimately leads to a stronger temperature profile. Fig. 10 indicates that the temperature profile is enhanced with an enhancement in the magnetic parameter M due to the presence of the Lorentz force. The situation when $M \neq 0$ represents the hydromagnetic flow and $M = 0$ depicts the hydrodynamic flow. It is quite evident that the temperature profile is higher for the hydromagnetic case as compared with the hydrodynamic case. The behavior of the thermophoresis parameter has been discussed in Fig. 11, where a rise in the thermophoresis parameter N_t seems to rise the fluid temperature. The reason behind the rise in temperature is an increment in the nanoparticles. It is observed that the nanoparticles present close to the hot boundary have been shifted towards the cold fluid in the presence of the thermophoretic force, thats why the thermal boundary layer becomes thicker. Fig. 12 shows the impact of the Prandtl number on the temperature profile. When the Prandtl number increases, a decrease in the thermal conductivity takes place and as a result the temperature profile decreases. Fig. 13 shows that an increment in the thermal radiation parameter gives more heat to the fluid which results an increment in the temperature and the thermal boundary layer thickness. Fig. 14 displays the effect of variation of θ_w on the temperature profile. It is quite clear that the temperature increases with a decrease in the values of the temperature ratio parameter θ_w. Fig. 15 depicts that an increase in the Biot number γ results an increase in the temperature profile because when the Biot number increases, higher convection takes

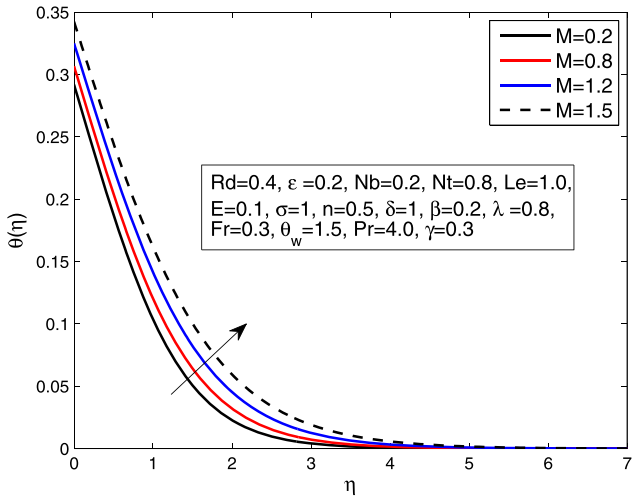

FIG. 10. Influence of M on θ.

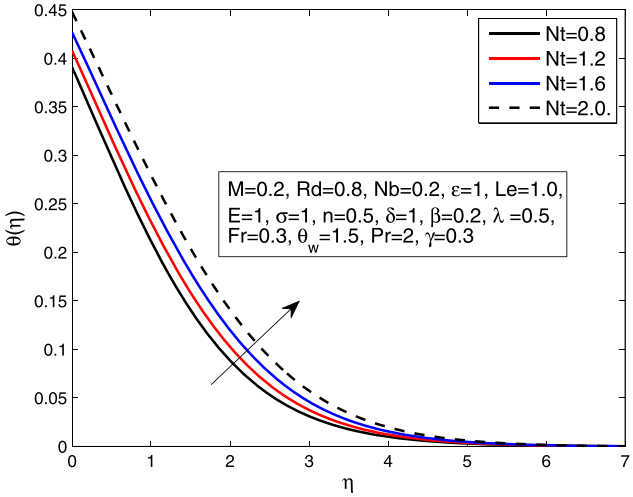

FIG. 11. Influence of N_t on θ.

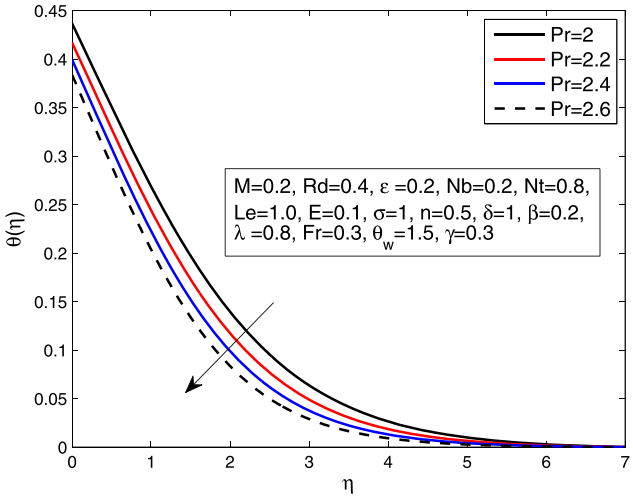

FIG. 12. Influence of Pr on θ.

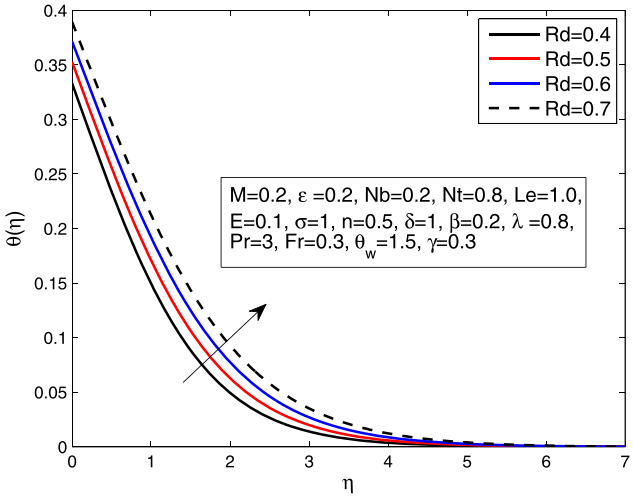

FIG. 13. Influence of Rd on θ.

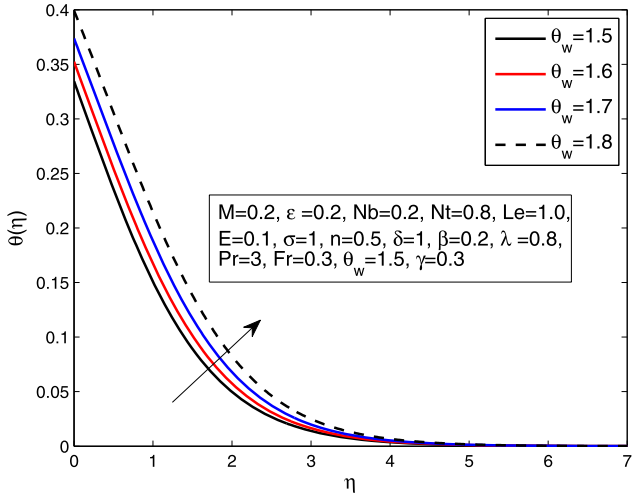

FIG. 14. Influence of θ_w on θ.

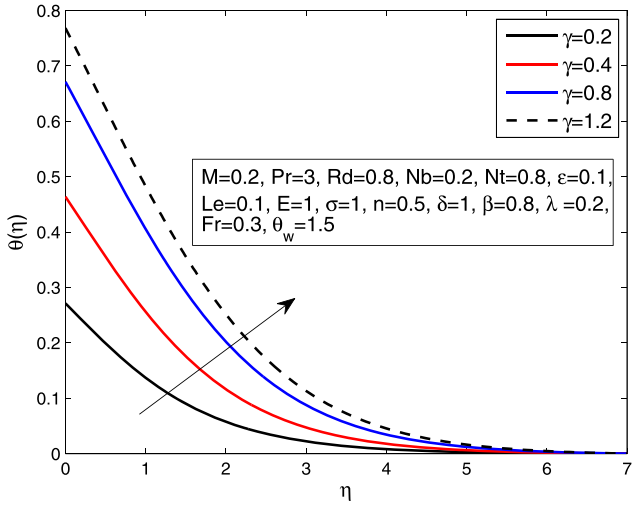

FIG. 15. Influence of γ on θ.

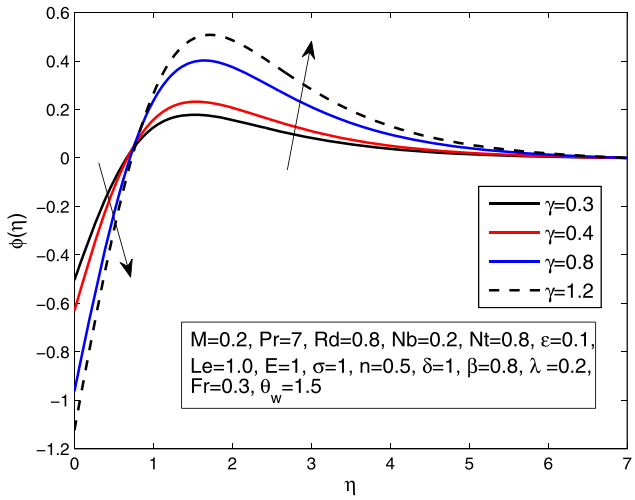

FIG. 16. Influence of γ on ϕ.

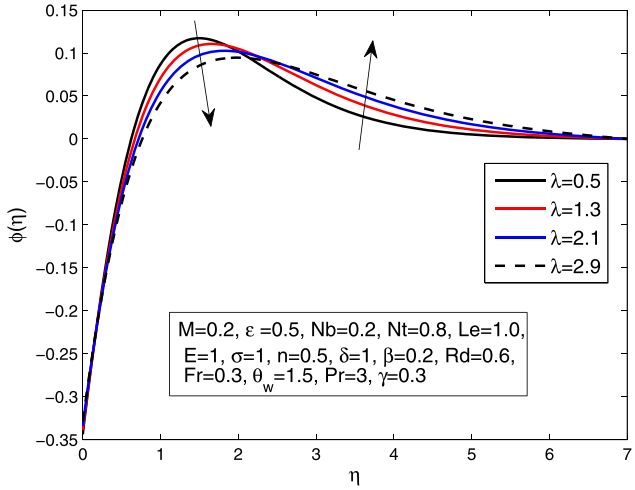

FIG. 17. Influence of λ on ϕ.

place which results in an increment in the temperature profile and thickness of the thermal boundary layer. The plot of the Biot number γ against the concentration profile is displayed in Fig. 16. When the Biot number increases, the value of the concentration profile and the thickness of concentration layer also increase. In Fig. 17, an increase in the porosity parameter λ, is found to result an increase in the concentration profile and thickness of the concentration boundary layer. Fig. 18 exhibits the variation of the nanoparticle concentration profile subject to the Lewis number for linear stretching sheet. Both the Lewis number and the Brownian diffusion coefficient are inversely related. It is analyzed that by increasing the value of the Lewis number, a decrease in the Brownian diffusion coefficient is observed, which results in a decrement in the nanoparticle concentration and the concentration boundary layer thickness. An increase in the values of the thermophoresis parameter results an increment in the temperature differences and the shear gradient. When the thermophoresis parameter increases, we expect a severe diffusion of nanoparticles in the base fluid. It causes the concentration boundary layer to rise for higher value of η as shown in Fig. 19. In the occurrence of thermophoresis, the little particles pushed far from hot surface towards the cold surface. It is researched that by enlarging the estimation of thermophoresis parameter directs to an augmentation in the nanoparticle concentration

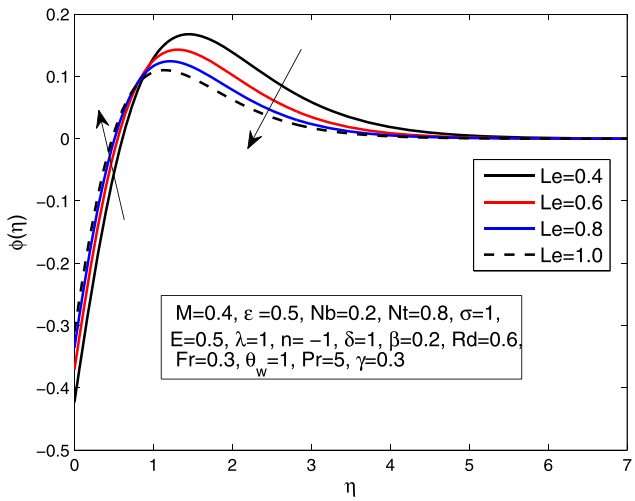

FIG. 18. Influence of *Le* on ϕ.

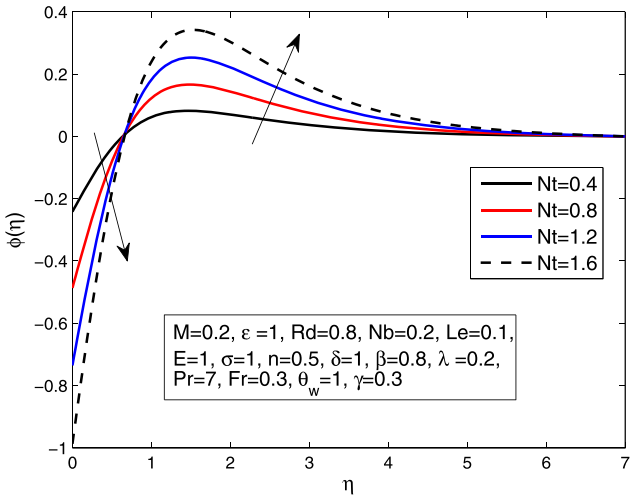

FIG. 19. Influence of N_t on ϕ.

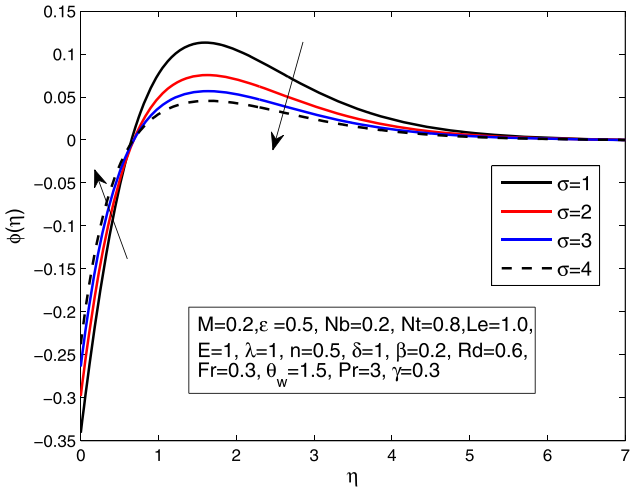

FIG. 20. Influence of σ on ϕ.

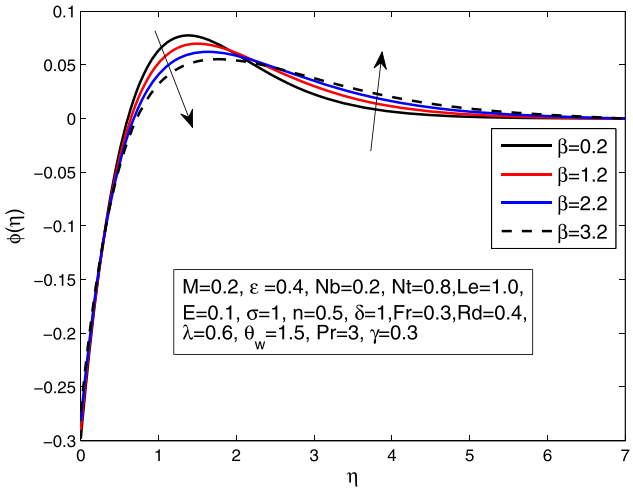

FIG. 21. Influence of β on ϕ.

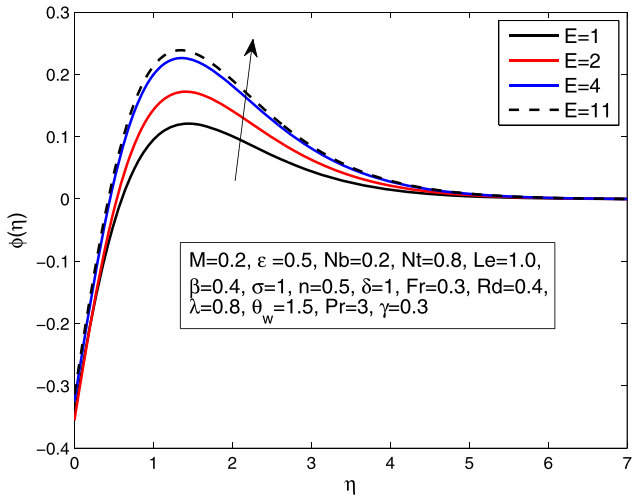

FIG. 22. Influence of E on ϕ.

profile. Fig. 20 indicates the behavior of the nanoparticle concentration for the reaction rate constant. It is clear that an increase in the chemical reaction parameter σ results in a decrement of nanoparticle concentration. When we upgrade the value of reaction rate parameter σ brings about an augmentation in the term $\sigma\,(1+\delta\theta)^n \exp\left(\frac{-E}{1+\delta\theta}\right)$. This inevitably leads to a destructive chemical reaction. Due to this concentration profile rises. Impact of Deborah number against concentration profile is portrayed in Fig. 21. It is obsecued that for higher value of ratio of relaxation to retardation time give ascent to the concentration field, yet reverse in the case of littler value of relaxation time to retardation time brings about decrement of the concentration profile. Fig. 22 explores the behavior of the activation energy against the nanoparticle concentration profile. The Arrhenius function decays by increasing the value of the activation energy, which results in the promotion of the generative chemical reaction causing an augmentation in the concentration profile. Within the occurrence of low temperature and higher activation energy leads to a smaller reaction rate constant which slow down the chemical reaction. In this manner concentration of solute rises. On account of high temperature and low concentration leads to larger reaction rate constant σ, which speed up the chemical reaction. Accordingly concentration of solute diminishes.

V. FINAL REMARKS

The present investigation is carried out to analyze the magnetohydrodynamics (MHD) stretched flow of Maxwell nanofluid with the convective boundary condition and consideration of some relevant physical parameters like activation energy, radiative heat flux and variable thermal conductivity. Some of the conclusive remarks for the present work are presented below.

- The velocity profile $f^{'}(\eta)$ show an opposite impact against the magnetic parameter M and inertia coefficient Fr.
- The temperature profile $\theta(\eta)$ has increasing behavior for the thermal conductivity ϵ, porosity parameter λ and Deborah number β.
- An increase in the thermophoresis parameter N_t, the radiation parameter Rd boosts the temperature profile $\theta(\eta)$.
- Large values of β and λ show an enhancing effect on the concentration profile $\phi(\eta)$ but opposite behaviour is observed in case of Le and σ.
- Rising the value of the Biot number γ results in an enhancement in both the velocity and the concentration profiles.
- Nusselt number decreases for boosting the value of thermophoresis parameter N_t.

- By increasing the variable thermal conductivity parameter, the heat transfer coefficient $-\theta'(0)$ decreases.
- A rise in the activation energy E decreases $-\theta'(0)$.
- A substantial increment in the radiation parameter Rd leads to an increase in $-\theta'(0)$.

[1] F. A. L. Dullien, *Porous Media*, Academic Press, San Diego (1992).
[2] D. A. Noeld and A. Bejan, *Convection in Porous Media* (Springer, New York, 1999).
[3] D. A. Noeld and A. Beskok, *Micro Flows* (Springer, New York, 2002).
[4] G. Karniadakis, A. Beskok, and N. Aluru, *Micro Flows and Nano Flows: Fundamentals and Simulation* (Springer, New York, 2005).
[5] P. Forchheimer, "Wasserbewegung Durch Boden," Zeitschrift des Vereins Deutscher Ingenieure **45**, 1782–1788 (1901).
[6] M. Muskat, *The flow of homogeneous fluids through porous media* (Edwards, Michigan, 1946).
[7] D. Pal and H. Mondal, "Hydromagnetic convective diffusion of species in Darcy-Forchheimer porous medium with non-uniform heat source/sink and variable viscosity," International Communication in Heat and Mass Transfer **39**, 913–917 (2012).
[8] N. V. Ganesh, A. K. A. Hakeem, and B. Ganga, "Darcy-Forchheimer flow of hydromagnetic nanofluid over a stretching/shrinking sheet in a thermally stratified porous medium with second order slip, viscous and Ohmic dissipations effects," Ain Shams Engineering Journal (2016).
[9] T. Hayat, T. Muhammad, S. Al-Mezal, and S. J. Liao, "Darcy-Forchheimer flow with variable thermal conductivity and Cattaneo-Christov heat flux," International Journal of Numerical Methods for Heat and Fluid Flow **26**, 2355–2369 (2016).
[10] T. Muhammad, A. Alsaedi, S. A. Shahzad, and T. Hayat, "A revised model for Darcy-Forchheimer flow of Maxwell nanofluid subject to convective boundary condition," Chinese Journal of Physics **55**, 963–976 (2017).
[11] J. Ahmed, A. Shahzad, M. Khan, and R. Ali, "A note on convective heat transfer of an MHD Jeffrey fluid over a stretching sheet," AIP Advances **5**, 117117 (2017).
[12] A. Alsaedi, F. E. Alsaadi, S. Ali, and T. Hayat, "Stagnation point flow of Burgers' fluid and mass transfer with chemical reaction and porosity," Journal of Mechanics **29**, 453–460 (2017).
[13] T. Aziz, F. M. Mahomed, A. Shahzad, and R. Ali, "Travelling wave solutions for the unsteady flow of a third grade fluid induced due to impulsive motion of flat porous plate embedded in a porous medium," Journal of Mechanics **30**, 527–535 (2017).
[14] A. Shahzad, R. Ali, and M. Khan, "On the exact solution for axisymmetric flow and heat transfer over a nonlinear radially stretching sheet," Chinese Physics Letters **29** (2012).
[15] S. U. S. Choi, "Enhancing thermal conductivity of fluids with nanoparticles," American Society of Mechanical Engineers **231**, 99–105 (1995).
[16] S. K. Das, S. U. S. Choi, W. Yu, and T. Pradeep, *Nanofluids: Science and Technology* (Wiley, New Jersey, 2007).
[17] X. Wang and A. S. Mujumdar, "A review model of nanofluids: Theoretical and numerical investigations," Brazilian Journal of Chemical Engineering **55**, 613–630 (2008).
[18] N. A. Usria, W. H. Azmi, R. Mamat, K. A. Hamid, and G. Najafi, "Thermal conductivity enhancement of Al_2O_3 nanofluid in ethylene glycol and water mixture," Energy Procedia **79**, 397–402 (2015).
[19] S. M. S. Murshed, K. C. Leong, and C. Yang, "Investigations of thermal conductivity and viscosity of nanofluids," International Journal of Thermal Sciences **47**, 560–568 (2008).
[20] J. Buongiorno, "Convective transport in nanofluids," ASME Journal of Heat Transfer **128**, 240–250 (2006).
[21] I. S. Oyelakin, S. Mondal, and P. Sibanda, "Unsteady Casson nanofluid flow over a stretching sheet with thermal radiation, convective and slip boundary conditions," Alexandria Engineering Journal **55**, 1025–1035 (2016).
[22] T. Hayat, M. Waqas, S. A. Shehzad, and A. Alsaedi, "Stretched flow of Carreau nanofluid with convective boundary condition," Pramana Journal of Physics **86**, 3–17 (1987).
[23] M. Bilal, M. Sagheer, and S. Hussain, "Three dimensional MHD upper-convected Maxwell nanofluid flow with nonlinear radiative heat flux," Alexandria Engineering Journal (2017).
[24] M. Bilal, M. Sagheer, and S. Hussain, "On MHD 3D upper convected Maxwell fluid flow with thermophoretic effect using non-linear radiative heat flux," Canadian Journal of Physics **96**(1), 1–10 (2017).
[25] M. Sheikholeslami, "CuO-water nanofluid free convection in a porous cavity considering Darcy law," The European Physical Journal Plus **55**, 132 (2017).
[26] M. M. Rashidi, Z. Yang, M. Awais, N. M. Nawaz, and T. Hayat, "Generalized magnetic field effects in Burgers nanofluid model," PLoS ONE **12**(1), e0168923 (2017).
[27] M. Kothandapani and J. Prakash, "Convective boundary conditions effect on peristaltic flow of a MHD Jeffery nanofluid," Applied Nanoscience **6**, 323–335 (2016).
[28] I. Ullah, S. Shafie, and I. Khan, "Effects of slip condition and Newtonian heating on MHD flow of Casson fluid over a nonlinearly stretching sheet saturated in a porous medium," Journal of King Saud University Science **29**, 250–259 (2017).
[29] S. A. Shehzad, T. Hayat, and A. Alsaedi, "Influence of convective heat and mass conditions in MHD flow of nanofluid," Bulletin of the Polish Academy of Sciences Technical Sciences **63**(2), 465–474 (2015).
[30] T. Hayat, M. Rashid, M. Imtiaz, and A. Alsaedi, "Magnetohydrodynamic (MHD) stretched flow of nanofluid with power-law velocity and chemical reaction," AIP Advances **5**, 117121 (2015).
[31] W. Ibrahim, "The effect of induced magnetic field and convective boundary condition on MHD stagnation point flow and heat transfer of upper-convected Maxwell fluid in the presence of nanoparticle past a stretching sheet," Propulsion and Power Research **5**, 164–175 (2016).
[32] N. A. Khan and S. Aziz, "Numerical simulation for the unsteady MHD flow and heat transfer of coupled stress fluid over a rotating disk," PLoS ONE **9**(5), e95423 (2014).

[33] A. Rauf, S. A. Shehzad, T. Hayat, M. A. Meraj, and A. AlSaedi, "MHD stagnation point flow of micro nanofluid towards a shrinking sheet with convective and zero mass flux conditions," Bulletin of the Polish Academy of Sciences Technical Sciences **65**(2), 155–162 (2017).
[34] R. Ali, A. Shahzad, M. Khan, and M. Ayub, "Analytic and numerical solutions for axisymmetric flow with partial slip," Engineering with Computers **32**, 149–154 (2016).
[35] A. Mushtaq, M. Mustafa, T. Hayat, and A. AlSaedi, "Nonlinear radiative heat transfer in the flow of nanofluid due to solar energy: A numerical study," Journal of the Taiwan Institute of Chemical Engineers **45**, 1176–1183 (2014).
[36] M. Monica and J. Sucharitha, "Effects of nonlinear thermal radiation, non-uniform heat source/sink on MHD stagnation point flow of a Casson fluid over a nonlinear stretching sheet with slip conditions," Journal of Nanofluids **6**, 692–701 (2017).
[37] B. Mahanthesh, B. J. Gireesha, and R. S. R. Gorla, "Nonlinear radiative heat transfer in MHD three-dimensional flow of water based nanofluid over a non-linearly stretching sheet with convective boundary condition," Journal of the Nigerian Mathematical Society **35**, 178–198 (2016).
[38] M. Bhatti, A. Zeeshan, and R. Ellahi, "Study of heat transfer with nonlinear thermal radiation on sinusoidal motion of magnetic solid particles in a dusty fluid," Journal of Theoretical and Applied Mechanics **46**, 75–94 (2016).
[39] N. S. Akbar, S. Nadeem, R. Ul Haq, and Z. H. Khan, "Radiation effects on MHD stagnation point flow of nanofluid towards a stretching surface with convective boundary condition," Chinese Journal of Aeronautics **26**, 1389–1397 (2013).
[40] M. Tencer, J. S. Moss, and T. Zapach, "Arrhenius average temperature: The effective temperature for non-fatigue wearout and long term reliability in variable thermal conditions and climates," IEEE Transactions on Components and Packaging Technologies **27**, 602–607 (2007).
[41] A. R. Bestman, "Radiative heat transfer to flow of a combustible mixture in a vertical pipe," International Journal of Energy Research **15**, 179–184 (1991).
[42] K. A. Maleque, "Effects of exothermic/endothermic chemical reactions with Arrhenius activation energy on MHD free convection and mass transfer flow in presence of thermal radiation," Journal of Thermodynamics **2013**, 1–11.
[43] Z. Shafique, M. Mustafa, and A. Mushtaq, "Boundary layer flow of Maxwell fluid in rotating frame with binary chemical reaction and activation energy," Results in Physics **6**, 627–633 (2016).
[44] M. Mustafa, A. Mushtaq, T. Hayat, and A. Alsaedi, "Numerical study of MHD viscoelastic fluid flow with binary chemical reaction and Arrhenius activation energy," International Journal of Chemical Reactor Engineering **15**, 627–633 (2016).
[45] K. Vajravelu and K. V. Prasad, "Unsteady convective boundary layer flow of a viscous fluid at a vertical surface with variable fluid properties," Nonlinear Analysis in Real World Application **14**, 455–464 (2013).
[46] B. R. Kumar and R. Sivaraj, "Heat and mass transfer in MHD viscoelastic fluid flow over a vertical plate with variable viscosity," International Journal of Heat and Mass Transfer **15**, 370–379 (2013).
[47] D. Pal and H. Mondal, "Effects of temperature-dependent viscosity and variable thermal conductivity on MHD non-Darcy mixed convective diffusion of species over a stretching sheet," Journal of Egyptian Mathematical Society **22**, 123–131 (2014).
[48] D. Pal and S. Chatterjee, "Soret and Dufour effects on MHD convective heat and mass transfer of a power-law fluid over an inclined plate with variable thermal conductivity in a porous medium," Applied Mathematics and Computation **219**, 7556–7574 (2013).
[49] T. Y. Na, *Computational Methods in Engineering Boundary Value Problems* (Academic Press, 1979), pp. 71–76.
[50] M. Bilal, S. Hussain, and M. Sagheer, "Boundary layer flow of magneto-micropolar nanofluid flow with Hall and ion-slip effects using variable thermal diffusivity," Bulletin of the Polish Academy of Sciences Technical Sciences **65**(3), 383–390 (2017).